Third order non-linear optical susceptibilities (χ 3) of yttria stabilized cubic hafnium(IV) oxide

Hassan Denawi, Jacques Demarais, C.S. Praveen, Michel Rérat, Panaghiotis Karamanis

THIRD ORDER NON-LINEAR OPTICAL SUSCEPTIBILITIES ($\chi^{(3)}$)OF YTTRIA STABILIZED CUBIC HAFNIUM(IV) OXIDE

HASSAN DENAWI[1], JACQUES K. DEMARAIS[1,2], C.S. PRAVEEN[3], MICHEL RERAT[1] AND PANAGHIOTIS KARAMANIS[1]*

[1]*E2S UPPA, CNRS, IPREM, Université de Pau et des Pays de l Adour, 64053 Pau, France*
[2] *International School of Photonics (ISP), Cochin University of Science and Technology (CUSAT), Kalamassery,Ernakulam, Cochin, Kerala, 682022, India*
[3]*Dipartimento di Chimica, Università di Torino, via Giuria 5, 10125 Torino, Italy blications Department*

**panagiotis.karamanis@gmail.com*

Abstract: This work reports for the first time theoretical third order nonlinear optical susceptibilities of YSH bulk phases which are key properties for telecommunication technologies and integrated photonic devices. Our outcomes, relying on coupled perturbed Kohn-Sham density functional theory expose that the NLO capacity of YSH should be similar to another material of this family, namely, yttria stabilized zirconia that has been proposed as a promising candidate for integrated photonics by Marcaud et al [Photon. Res. **8**, 110 (2020)]. Finally, evidence implying important vibrational contributions to the optical nonlinearities of the systems are revealed and analyzed.

1. Introduction

The key to harness light's nonlinear effects and to unlock its "limitless" potential in telecommunication technologies lies in the successful and cost-effective fabrication of fully operating integrated nonlinear photonic devices. [1,2] Upon success, ultra-fast optical processing at femtosecond time scales, having the capacity to give access to petahertz telecommunication bandwidths, could eventually be achieved. In this realm, one of the main properties of interest is the so called intrinsic third order non-linear optical (NLO) susceptibility, 3] routinely designated as $\chi^{(3)}$. The latter band-gap dependent property provides the means to control light with light, [4] via the so-called Kerr effect which reflects the ability of a given material to change its refractive index upon the application of an electric field. In this context, Marcaud *et al.* [5] reported the outcomes of a joint experimental and theoretical work dealing with the NLO behavior of yttria stabilized zirconia (YSZ). As demonstrated in that work ,YSZ, that can be grown epitaxially[6] on silicon substrates, features a comparable third order

nonlinear effective Kerr coefficient ($\hat{n}_2$) with silicon nitride.[7] The latter material although it is one of the materials of choice for integrated photonics it suffers from significant shortcomings due to strong two photon absorption (TPA) effects that induce significant optical losses (see ref [5] and references therein). As Marcaud *et al.* concluded, TPA loses in YSZ are expected to be negligible thanks to its large bandgap and its quasi-cubic local atomistic structure. [5]

Motivated by the intense technological interest in the optical properties of functional oxides for integrated photonic devices worldwide, in this article, we report on reliable $\chi^{(3)}$ estimations of another widely recognized functional oxide, namely, yttria stabilized hafnia (YSH). Hafnia (HfO_2),[8] the parent material of YSH, is known to possess four crystalline phases[9], namely, tetragonal, monoclinic, cubic and amorphous. Out of the four hafnia phases the third one (c-HfO_2) is of great interest in CMOS technologies owed to its high dielectric constant and wider band gap. [10] However, cubic hafnia becomes "functional" only in quite high temperatures (> 2500 ºC)[11] and this impedes its application in many areas including optoelectronics. Therefore, its stabilization at ambient conditions via doping is one of the preferred options. For this task, Y_2O_3 has proven a highly effective doping agent since it "stabilizes" hafnia's cubic phase even in relatively low concentrations ranging from 0.6 mol% to 6.5 mol%. In particular, the current work reports on accurate coupled perturbed electronic static $\chi^{(3)}_{iiii,iijj}$ macroscopic data defined as:

$$\chi^{(3)}_{iiii,iijj} = 2\pi\gamma^{e}_{iiii,iijj}(3V)^{-1} \text{ (where, i and j are the cartesian cell axes)}$$

In Eq. (1) γ^e is electronic contribution of the second hyperpolarizability per unit cell volume (V). The latter quantity can be determined experimentally[7] via measurements of the refractive

index: $\hat{n}_2 = 3\hat{\chi}^{(3)}(4c\epsilon_0\epsilon)^{-1}$ (ϵ is the relative dielectric in-plane ϵ_{xx} component, ϵ_0 the electric permittivity of vacuum and c the light velocity and $\hat{\chi}^{(3)}$ is the effective third order susceptibility[5]).

2. Results and discussion

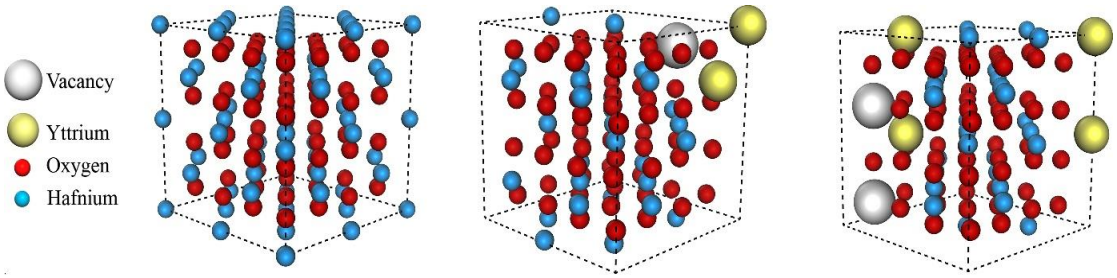

	HfO_2	HfO_2 3mol% Y_2O_3	HfO_2 7mol% Y_2O_3
Volume (Å^3)	1021	1035	1043
Lattice const. (Å)	a,b,c=10.07	a=10.14 b,c=10.10	a=10.26 b,c=10.22
Dielectric components	$\epsilon_{xx,yy,zz}$=3.84	ϵ_{xx}=3.57 $\epsilon_{yy,zz}$=3.75	ϵ_{xx}=4.11 $\epsilon_{yy,zz}$=4.14

Fig. 1. Relaxed stoichiometric atomistic super-cells YSH. All structures are true minima of the corresponding supercell potential energy super-surfaces.

All computations presented and discussed here have been carried out using widely tested density functional methods (DFT) as implemented in CRYSTAL17 code. [11] In brief, the generalized gradient approximation (GGA) functional of Perdew, Burke, and Ernzerhof (PBE) and the hybrid functionals PBE0 and B3LYP, have been employed to check the method dependence on the properties of interest. A supercell size of 2 × 2 × 2 has been considered for the disordered and vacancy calculations with a corresponding Monkhorst-Pack grid [12] of 8 × 8 × 8. The spatial doping/vacancy distribution chosen has been based on earlier benchmark computations initially carried out on YSZ [5] and applied here on YSH. Although our structural investigation is not exhaustive, our experience on YSZ [5] phases suggests that there is a minor influence of the local atomistic structures of such oxides on the electronic part of their third

order nonlinearities which is expected to dominate the overall response. The computation of the linear and nonlinear properties addressed here relied on coupled perturbed Kohn-Sham density functional theory as implemented [13] in CRYSTAL 17 by one of the authors of this study. For Y and Hf atoms, we relied on pseudo-potential (ECP) basis set constructed by Hay–Wadt and Stevens *et al*., respectively [14,15] For O atoms, the Durand–Barthelat[16] ECP basis set was chosen in which the $1s^2$ core electrons are approximated by a nonrelativistic potential.

Table 1. Energy Band Gaps (Eg, in eV) of HfO_2, YSH and YSZ, obtained within a plane wave and crystalline orbital calculations.

	PBE	PBE0	B3LYP
c-HfO_2	4.04	6.47	6.03
3.2%YSH	4.38	6.77	6.26
6.7%YSH	4.56	6.98	6.45
6.7%YSZ	3.58	5.83	5.39

The relaxed stoichiometric atomistic super-cell structure of c-HfO_2 (2×2×2) as well as two cells of YSH of the same size containing 3.2 and 6.7 mol% of Y_2O_3, (hereafter (3.2%,6.7%) YSH), considered in this report are illustrated in **Fig. 1**. Our structural results for c-HfO_2, also shown in the latter figure, are in good agreement with previously theoretical and experimental outcomes reported by Zhao and Vanderbilt [17] within the local density and generalized gradient approximation and close to the experimental value [18] of 5.08 Å per unit cell (10.16 Å for a 2×2×2 supercell). According to our knowledge up until now, no experimental or theoretical structural data have been reported for either concentration of YSH.

The energy bandgap values of the above compositions, computed with a pure DFT functional (PBE), and two different hybrid functionals (PBE0, B3LYP), are presented in **Table**

92 **1**. As expected, PBE functional, the least expensive computational method used here in, delivers
93 considerably smaller bandgaps with respect to the two hybrids PBE0 and B3LYP. A direct
94 comparison of our computed band gap of c-HfO_2 with spectroscopic ellipsometry
95 measurements of 5.8 eV reported by C. Adelmann *et al.* [19] reveals that the two hybrids, PBE0
96 and B3LYP, predict considerably improved bandgap energies lying about 0.7 and 0.2 eV above
97 the experiment, respectively. We expect similar method behavior for YSH phases considered
98 in this work.

99 As far as it concerns the dependence of YSH bandgap on the doping concentration,
100 our computational outcomes, clearly suggest that doping c-HfO_2 with yttrium induces a
101 noticeable bandgap broadening. The observed evolution is in accord with the trend reported
102 by Chen *et al* [20] who studied the dependence of Y_2O_3 concentration on the optical properties
103 of crystalline HfO_2 thin films via spectroscopic ellipsometry and concluded to a proportional
104 dependence of the measured band gaps with respect to the doping concentration. Spin-orbit-
105 coupling effects (SOC) on the band structures of pure and doped hafnia using richer basis sets
106 [21, 22, 23, 24]. for all atoms have been considered by applying a newly developed scheme in
107 CRYSTAL based on two-component spin-current density functional theory [25,26]. In brief, For Y
108 and Hf we used a fully relativistic effective core potential (ECP) including both the scalar-
109 relativistic AREP and the spin-orbit SOREP parts, developed by Peterson *et al*. [27] and
110 Figgen *et al*.[28]. For Y, an associated valence basis set of triple-zeta quality was available for
111 solid-state calculations reported by Laun *et al*.[29] In the case of Hf, the basis set applied was
112 derived from the associated correlation-consistent double-zeta set for molecular calculations
113 provided by Peterson *et al*.[24] after we uncontracted the set and removed Gaussians with
114 exponents smaller than 0.1 a.u to avoid linear dependencies. Our final uncontracted Hf valence

115 basis set is available at CRYSTAL basis set library [30] For O we used the basis set from
116 Heifets et al. [31]

117 The computations, carried out on the optimized supercells of **Fig. 1**, exposed that SOC brings
118 minor corrections on the band gaps of all systems considered. Specifically, for pure c-HfO_2
119 SOC increases the respective band gap by 0.004 eV while in the case of 3.2% and 6.7% YSH
120 a bandgap opening by 0.007 and 0.006 eV is delivered, respectively. Furthermore, as it can be
121 easily seen in **Fig. 2**, where we depict the total (DOS) and projected (PDOS) density of states
122 of 3.2% YSH, the weak spin-orbit-coupling effects evidenced in the band splitting is transferred
123 also on the shape and intensity of the computed DOS and PDOS spectra.

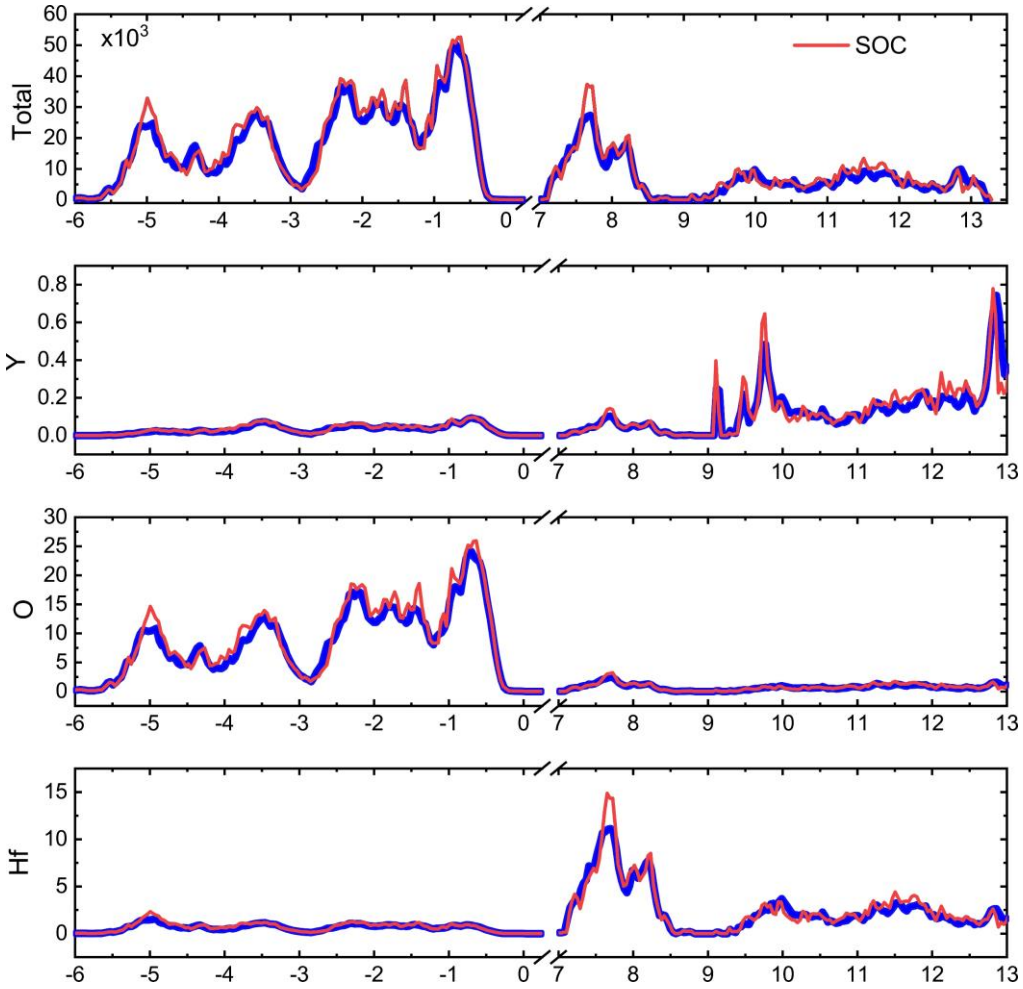

Fig. 2. Total and projected densities of states for 3.2% YSH obtained at the PBE0. Red colored (P)DOSS spectra correspond to computations considering spin-orbit-couplings (SOC).

Table 2. Electronic contribution to the dielectric $\epsilon_{xx}, \epsilon_{yy=zz}$ components, to the third order susceptibilities $\chi^{(3)}_{xxxx}$, $\chi^{(3)}_{yyyy=zzzz}$, $\chi^{(3)}_{yyzz}$components$\left(\times 10^{-21} m^2 V^{-2}\right)$, of HfO_2, YSH 3.2% and 6.7% mol.in Y_2O_3 and YSZ 6.7% mol. in Y_2O_3. In this case *x*, y and *z* are placed parallel to the lattice constants a, b and c, respectively.

		$\epsilon_{xx} = \epsilon_{yy} = \epsilon_{zz}$		$\chi^{(3)}_{xxxx} = \chi^{(3)}_{yyyy} = \chi^{(3)}_{zzzz}$		$\chi^{(3)}_{yyzz}$
c-HfO_2	PBE0	3.8		0.9		0.7
	B3LYP	3.9		1.1		0.8
		$\epsilon_{xx} = \epsilon_{yy}$	ϵ_{zz}	$\chi^{(3)}_{xxxx}$	$\chi^{(3)}_{yyyy} = \chi^{(3)}_{zzzz}$	$\chi^{(3)}_{yyzz}$
3.2%YSH	PBE0	3.6	3.7	0.7	0.8	0.6
	B3LYP	3.7	3.8	0.9	0.9	0.7
6.7%YSH	PBE0	3.5	3.7	0.6	0.7	0.6
	B3LYP	3.6	3.8	0.8	0.9	0.6
6 .7%YSZ	PBE0	4.1	4.14	1.2	1.2	1.0
	B3LYP	4.2	4.25	1.5	1.4	1.2

Let us now turn our attention to **Table 2** that summarizes our analytical CPKS outcomes of the dielectric components and the electronic part of the third order NLO susceptibilities of undoped hafnia, 3.2%, 6.7%YSH and 6.7%YSZ. Starting from the relative dielectric tensorial components we see that yttrium doping delivers a slight anisotropy with respect to the perfect cubic phase. This trend is also followed by the computed third-order susceptibilities. Moving now to the properties of interest we see that for all systems both functionals yield third-order susceptibilities not far from the limit of $10^{-21} m^2 V^{-2}$ which is considered adequate for certain photonic applications [5]. In addition, it becomes evident that yttrium doping delivers a slight decrease in $\chi^{(3)}_{yyyy}$, $\chi^{(3)}_{zzzz}$ and $\chi^{(3)}_{yyzz}$ components, a result that is in accord with the evident

bandgap widening occurring upon Y doping due to the inverse proportionality of $\chi^{(3)}$ to the bandgap of a given material. If we now directly compare the third order nonlinearities of 6.7%YSH to its zirconia analogue, that in this case shares the same local atomistic structure, it is revealed that both lattices feature $\chi^{(3)}$ values of a similar order of magnitudes with the latter being about two times more hyperpolarizable than the former. The revealed ordering is in accord with the wider band gap values of YSH. Furthermore, to facilitate the comparison with previous, and more importantly, future experimental measurements for similar systems, we have used the tensorial components shown in **Table 2** to calculate the effective Kerr coefficient $\hat{n}_2$ of and as shown by Marcaud *et al.*[5] The obtained outcome of 0.8×10^{-19}m^{2}W^{-1} for 6.7%YSH at B3LYP level, lies about 1.6 times lower than the effective Kerr coefficient of 6.7%YSZ obtained at the same level of theory.

Bearing in mind that the nonlinearities discussed so far correspond to the electronic part of $\chi^{(3)}$, one should regard the nonlinear coefficients listed in **Table 2** as the lowest limit at each level of theory. Based on previous results for YSZ, we expect that the actual NLO response of YSH should be even stronger owed to a combination of effects related to the frequencies of the applied dynamic or oscillating electric fields (c.c. frequency dispersion), possible thermal lattice expansions, and more importantly to vibrational contributions.[32] To address the latter effects we relied on the variation of the dipole polarizability of each unit cell with respect to the atomic displacement along the axial supercell directions. For this task, we applied the formulation corresponding to one of the most common NLO processes, namely, the intensity-dependent refractive index (IDRI). In this process and by means of the so-called infinite-frequency approximation, [33] the harmonic diagonal vibronic contribution is simplified as:

$$\gamma^{vib}_{xxxx,yyyy,zzzz} \simeq 2\sum_{k=1}^{3N-3} \frac{\left(\frac{\vartheta \alpha^{e}_{xx,yy,zz}}{\vartheta Q_k}\right)^2}{\omega_k^2} \quad (2)$$

In Eq. (2) N is the number of atomic centers comprised in the unit cell and $\frac{\vartheta \alpha^{e}_{xx,yy,zz}}{\vartheta Q_k}$ the derivative of the axial dipole polarizability component per unit cell with respect to the harmonic normal Q_k-mode with ω_k-frequency. The obtained analytical outcomes within the CPKS approximation are presented in **Table 3** and reveal that for pristine hafnia the vibrational contributions are extremely weak with respect to the electronic ones. In striking contrast, our computations at the PBE0 level expose a strong vibrational contribution of 3.0×10^5 and 3.2×10^5 a.u. along the *x*-axis of the unit cells of 3.2%YSH and 6.7%YSH, respectively. As a result, a γ^{tot}_{xxxx} value of 9.5×10^5 a.u. which lies about 1.5 times higher than the corresponding γ^{e}_{xxxx} value of 3.2%YSH, has been obtained. A similar behavior is observed for 6.7%YSH.

Taking into consideration that the computed RAMAN intensities are proportional to the square of the first derivative of the dipole polarizability with respect to the corresponding displacement mode, the revealed vibrational effects can be rationalized up to a great extent by a careful analysis of the simulated RAMAN spectra shown in **Figure 3**. Thereby, we see that the spectrum of pure cubic hafnia is characterized by a single strong absorption band at 640cm^{-1}. Despite its large intensity, the respective absorption band lies too high in energy to induce strong vibrational contributions to the second dipole hyperpolarizability along any Cartesian cell direction. On the other hand, in the RAMAN spectra of the two YSH phases one can easily spot several soft active absorption bands appearing in low energies. Their origin should be attributed to the weak but evident deviation from the cubic symmetry of the doped YSH supercell due to the replacement of two

Table 3. Unit cell electronic (γ^{e}), vibrational (γ^{vib}), and total ($\gamma^{tot} = \gamma^{e}+\gamma^{vib}$) second dipole hyperpolarizability axial tensorial components of c-HfO_2 and YSH, respectively, computed with the PBE0 functional. All values are given in atomic unit and have been at the PBE0 level of theory applying the same basis sets we used for the geometry optimization.

c-HfO_2	γ^{e}_{xxxx} γ^{e}_{yyyy} γ^{e}_{zzzz}	7.9×10^{5}	γ^{vib}_{xxxx} γ^{vib}_{yyyy} γ^{vib}_{zzzz}	~0	γ^{tot}_{xxxx} γ^{tot}_{yyyy} γ^{tot}_{zzzz}	7.9×10^{5}
3.2%YSH	γ^{e}_{xxxx}	6.5×10^{5}	γ^{vib}_{xxxx}	3.0×10^{5}	γ^{tot}_{xxxx}	9.5×10^{5}
	γ^{e}_{yyyy},γ^{e}_{zzzz}	7.1×10^{5}	γ^{vib}_{yyyy},γ^{vib}_{zzzz}	0.2×10^{5}	γ^{tot}_{yyyy},γ^{tot}_{zzzz}	7.3×10^{5}
6.7%YSH	γ^{e}_{xxxx}	5.8×10^{5}	γ^{vib}_{xxxx}	3.2×10^{5}	γ^{tot}_{xxxx}	9.0×10^{5}
	γ^{e}_{yyyy},γ^{e}_{zzzz}	6.5×10^{5}	γ^{vib}_{yyyy},γ^{vib}_{zzzz}	0.3×10^{5}	γ^{tot}_{yyyy},γ^{tot}_{zzzz}	6.8×10^{5}

Hf atoms with Yttria and the creation of an oxygen vacancy. This structural distortion, clearly expressed by an elongated lattice constant a (see **Fig. 1**), activates several soft RAMAN active absorption bands that potentially could contribute in an additive manner to the supercell's second hyperpolarizabilities. In the present case, the vibrational contributions appear considerably strong in the direction of the most anisotropic tensorial componentγ^{e}_{xxxx} ($\neq \gamma^{e}_{yyyy} \cong \gamma^{e}_{zzzz}$) which, in turn, corresponds to the most distorted lattice constant **a** (note that in the current case lattice constants **a**, **b** and **c** coincide with the *x*, *y* and *z* axes, respectively). Indeed, as seen by the values listed in **Table 3**, γ^{vib}_{xxxx} appears about fifteen and ten times greater than γ^{vib}_{yyyy} and γ^{vib}_{zzzz}or either 3.2% or 6.7% YSH, respectively. Finally, as seen by the displacement modes depicted in **Fig. 3** the low frequency acoustic modes which play a central role in the respective

vibrational contribution are in fact a mixture of antisymmetric oxygen displacements. For instance, at the PBE0 level of theory the contribution of the mode highlighted for 3.2%YSH contributes up one third (~ 1.0×10^5 au) of the overall γ^{vib}_{xxxx} value.

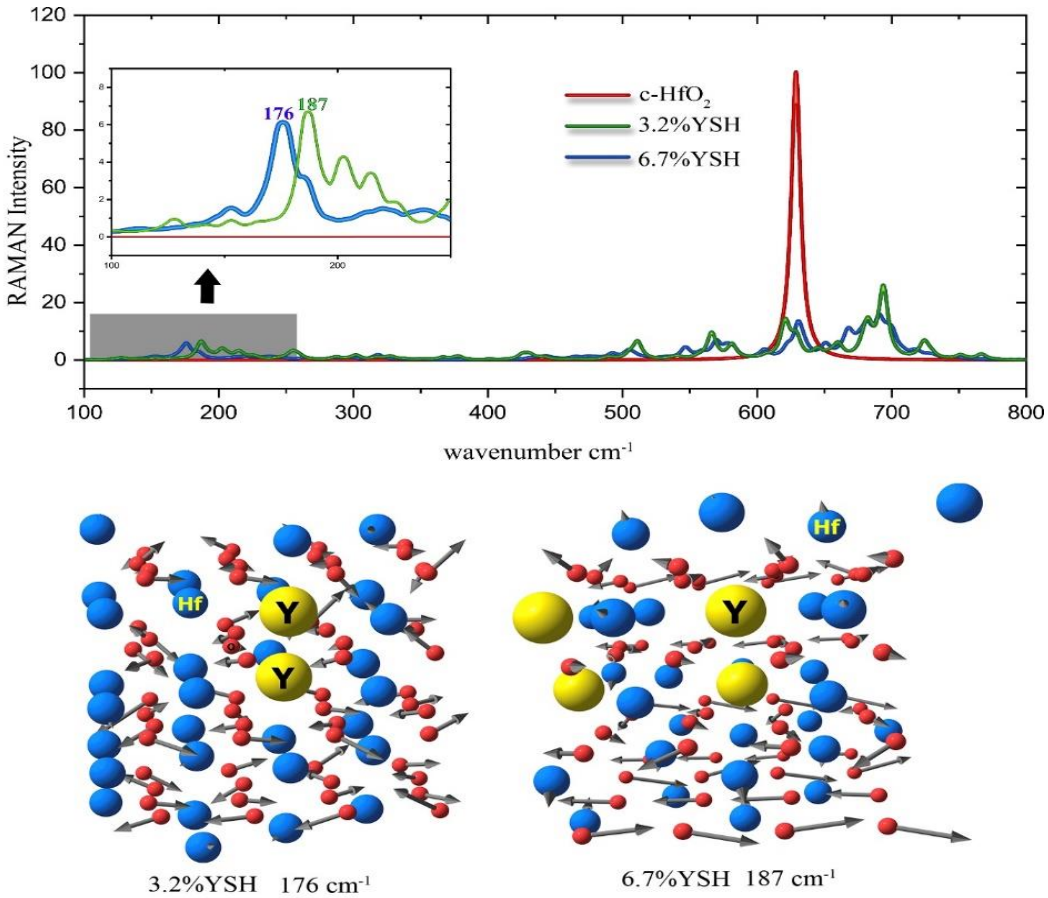

Fig.3. RAMAN spectra of 3.2%YSH and 6.7%YSH (right) and computed displacement vectors of soft vibrational modes contributing the most on the vibrational supercell hyperpolarizabilities. All computations have been permed at the PBE0 level of theory.

3. Conclusion

In this work, the structural, electronic, and optical properties of cubic HfO_2 and YSH bulk have been investigated by first-principles calculations. Our computational data suggest that the NLO capacity of YSH, should be comparable to YSZ recently studied both experimentally and theoretically by Marcaud *et al*. In addition, by applying a newly developed method, recently

implemented in CRYSTAL17, it has been exposed that the electronic properties of YSH do not constitute subjects of strong spin orbit coupling effects. Finally, strong evidence of significant vibrational contributions to the optical nonlinearities of the systems have been found. An article addressing in more details these effects is in preparation.

Acknowledgments

Part of this work was granted access to the HPC resources of [CCRT/CINES/IDRIS] under the allocations 2019-2020 2020-2021 [A0040807031] made by GENCI (Grand Equipement National de Calcul Intensif). We also acknowledge the “Direction du Numérique” of the “Université de Pau et des Pays de l’Adour” and the Mésocentre de Calcul Intensif Aquitain (MCIA) for the computing facilities provided. H. Denawi thanks ANR project FOIST. CSP acknowledges DST-India for INSPIRE Faculty Fellowship with award number IFA-18 PH217. JKD is grateful to the national science and engineering research council (NSERC) for a postdoctoral fellowship No. 545643. The authors declare that they have no known competing financial interest.

References

1. A. B. Miller, "Are optical transistors the logical next step?," Nature Photon **4**, 3–5 (2010)
2. S. M. Hendrickson, A. C. Foster, R. M. Camacho, and B. D. Clader, "Integrated nonlinear photonics: emerging applications and ongoing challenges," J. Opt. Soc. Am. B **31**, 3193 (2014).
3. R. W. Boyd, *Nonlinear Optics* (Academic Press, San Diego, CA, 1992)
4. M. G. Kuzyk, "Connecting at the speed of light," IEEE Circuits and Devices Magazine **19**, 8–17 (2003).
5. G. Marcaud, S. Serna, P. Karamanis, C. Alonso-Ramos, X. Le Roux, M. Berciano, T. Maroutian, G. Agnus, P. Aubert, A. Jollivet, A. Ruiz-Caridad, L. Largeau, N. Isac, E. Cassan, S. Matzen, N. Dubreuil, M. Rérat, P. Lecoeur, and L. Vivien, "Third-order nonlinear optical susceptibility of crystalline oxide yttria-stabilized zirconia," Photon. Res. **8**, 110 (2020).
6. S. K. Pandey, O. P. Thakur, R. Raman, A. Goyal, and A. Gupta, "Structural and optical properties of YSZ thin films grown by PLD technique," Applied Surface Science **257**, 6833–6836 (2011).
7. D.J. Moss, R. Morandotti, A.L. Gaeta, and M. Lipson, "New CMOS-compatible platforms based on silicon nitride and Hydex for nonlinear optics," Nature Photon **7**, 597 (2013).

8. J. Robertson, "High dielectric constant gate oxides for metal oxide Si transistors," Rep. Prog. Phys. **69**, 327–396 (2006).
9. O. Ohtaka, H. Fukui, T. Kunisada, T. Fujisawa, K. Funakoshi, W. Utsumi, T. Irifune, K. Kuroda, and T. Kikegawa, "Phase Relations and Volume Changes of Hafnia under High Pressure and High Temperature," Journal of the American Ceramic Society **84**, 1369–1373 (2004).
10 J. H. Choi, Y. Mao, and J. P. Chang, "Development of hafnium based high-k materials—A review," Materials Science and Engineering: R: Reports **72**, 97–136 (2011)..
11. R. Dovesi, A. Erba, R. Orlando, C.M. Zicovich-Wilson, B. Civalleri, L. Maschio, M. Rérat, S. Casassa, J. Baima, S. Salustro, and B. Kirtman, WIREs Computational Molecular Science **8**, e1360 (2018).
12. H. J. Monkhorst and J. D. Pack, "Special points for Brillouin-zone integrations," Phys. Rev. B **13**, 5188–5192 (1976)
13. M. Ferrero, M. Rérat, B. Kirtman, and R. Dovesi, "Calculation of first and second static hyperpolarizabilities of one- to three-dimensional periodic compounds. Implementation in the CRYSTAL code.," J. Chem. Phys. **129**, 244110 (2008).
14. P. J. Hay and W. R. Wadt, "Ab initio effective core potentials for molecular calculations. Potentials for the transition metal atoms Sc to Hg," J. Chem. Phys. **82**, 270–283 (1985).
15. W. J. Stevens, M. Krauss, H. Basch, and P. G. Jasien, "Relativistic compact effective potentials and efficient, shared-exponent basis sets for the third-, fourth-, and fifth-row atoms," Can. J. Chem. **70**, 612–630 (1992).
16. J. C. Barthelat, P. Durand, and A. Serafini, "Non-empirical pseudopotentials for molecular calculations," Molecular Physics **33**, 159–180 (1977).
17. 1. X. Zhao and D. Vanderbilt, "First-principles study of structural, vibrational, and lattice dielectric properties of hafnium oxide," Phys. Rev. B **65**, 233106 (2002).
18. J. Wang, H. P. Li, and R. Stevens, "Hafnia and hafnia-toughened ceramics," J Mater Sci **27**, 5397–5430 (1992).
19. C. Adelmann, V. Sriramkumar, S. Van Elshocht, P. Lehnen, T. Conard, and S. De Gendt, "Dielectric properties of dysprosium- and scandium-doped hafnium dioxide thin films," Appl. Phys. Lett. **91**, 162902 (2007).
20. X. Chen, L. Song, L. You, and L. Zhao, "Incorporation effect of Y2O3 on the structure and optical properties of HfO2 thin films," Applied Surface Science **271**, 248–252 (2013).
21. K. A. Peterson, D. Figgen, M. Dolg, and H. Stoll, "Energy-consistent relativistic pseudopotentials and correlation consistent basis sets for the 4d elements Y–Pd," J. Chem. Phys. **126**, 124101 (2007).
22. D. Figgen, K. A. Peterson, M. Dolg, and H. Stoll, "Energy-consistent pseudopotentials and correlation consistent basis sets for the 5d elements Hf–Pt," J. Chem. Phys. **130**, 164108 (2009).
23. J. Laun, D. Vilela Oliveira, and T. Bredow, "Consistent gaussian basis sets of double- and triple-zeta valence with polarization quality of the fifth period for solid-state calculations," J Comput Chem **39**, 1285–1290 (2018).
24. E. Heifets, E. A. Kotomin, A. A. Bagaturyants, and J. Maier, "Thermodynamic stability of non-stoichiometric SrFeO3−δ: a hybrid DFT study," Phys. Chem. Chem. Phys. **21**, 3918–3931 (2019).
25. J. K. Desmarais, J.-P. Flament, and A. Erba, "Spin-orbit coupling in periodic systems with broken time-reversal symmetry: Formal and computational aspects," Phys. Rev. B **101**, 235142 (2020).
26. J. K. Desmarais, S. Komorovsky, J.-P. Flament, and A. Erba, "Spin–orbit coupling from a two-component self-consistent approach. II. Non-collinear density functional theories," J. Chem. Phys. **154**, 204110 (2021).

27 K. A. Peterson, D. Figgen, M. Dolg, and H. Stoll, "Energy-consistent relativistic pseudopotentials and correlation consistent basis sets for the 4d elements Y–Pd," J. Chem. Phys. **126**, 124101 (2007).
28. D. Figgen, K. A. Peterson, M. Dolg, and H. Stoll, "Energy-consistent pseudopotentials and correlation consistent basis sets for the 5d elements Hf–Pt," J. Chem. Phys. **130**, 164108 (2009).
29.J. Laun, D. Vilela Oliveira, and T. Bredow, "Consistent gaussian basis sets of double- and triple-zeta valence with polarization quality of the fifth period for solid-state calculations," J Comput Chem **39**, 1285–1290 (2018).
30 www.crystal.unito.it/Basis_Sets/hafnium.html
31 E. Heifets, E. A. Kotomin, A. A. Bagaturyants, and J. Maier, "Thermodynamic stability of non-stoichiometric SrFeO3−δ: a hybrid DFT study," Phys. Chem. Chem. Phys. **21**, 3918–3931 (2019).
32. D. M. Bishop, J. M. Luis, and B. Kirtman, "Vibration and two-photon absorption," The Journal of Chemical Physics **116**, 9729–9739 (2002).
33. B. Champagne, É. A. Perpète", J.-M. André, and B. Kirtman, "Analysis of the vibrational static and dynamic second hyperpolarizabilities of polyacetylene chains," Synthetic Metals **85**, 1047–1050 (1997).